communications earth & environment

Article

https://doi.org/10.1038/s43247-024-01965-9

Organic ligands in whale excrement support iron availability and reduce copper toxicity to the surface ocean

Patrick J. Monreal[1,2] ✉, Matthew S. Savoca[3], Lydia Babcock-Adams[4], Laura E. Moore[1], Angel Ruacho[1], Dylan Hull[1], Logan J. Pallin[5], Ross C. Nichols[5], John Calambokidis[6], Joseph A. Resing[1,7,8], Ari S. Friedlaender[5], Jeremy Goldbogen[3] & Randelle M. Bundy[1] ✉

Nutrient recycling by marine megafauna is a key ecosystem service that has been disturbed by anthropogenic activity. While some hypotheses attribute Southern Ocean ecosystem restructuring to disruptions in micronutrient cycling after the elimination of two million great whales, there is little knowledge of trace metal lability in whale excrement. Here we measured high concentrations of dissolved iron and copper in five baleen whale fecal samples and characterized micromolar levels of organic metal-binding ligands as a proxy for their availability. The iron-ligand pool consisted of weakly-binding ligands and intermediate-binding ligands which enhanced iron stability and potential bioavailability. In comparison, 47 novel strongly-binding metallophores dominated copper-binding, curtailing its potential toxicity. These results illustrate how marine megafauna transform prey biomass into highly-labile micronutrients that they inject directly into the surface ocean, a mechanism whaling reduced by over 90%. Thus, the rapid restructuring of pelagic ecosystems through overharvesting may cause large biogeochemical feedbacks, altering primary productivity and carbon sequestration processes in the ocean.

Trace metals are vital micronutrients to marine life with vanishingly-small concentrations in surface seawater, making them crucial controls on many biogeochemical processes. Primary production in large swaths of the ocean is limited by the key micronutrient iron (Fe), despite relatively high amounts of upwelled macronutrients (e.g., nitrogen and phosphorous)[1,2]. These high-nutrient low-chlorophyll (HNLC) areas exist due to their remoteness from continental Fe sources and the low solubility of Fe in seawater[3–5]. Copper (Cu) is also necessary for several biological functions like electron transport and Fe uptake[6] but can be toxic at just picomolar concentrations in cultures[7]; this dichotomy gives Cu a crucial role in shaping microbial community composition[8]. Some organisms, like ammonia-oxidizing archaea[9] and certain diatoms whose growth is limited by Fe, have large Cu requirements, intertwining the cycling of Fe and Cu in HNLC regions[10]. In the context of Earth's changing climate and interest in marine carbon dioxide removal strategies, there is strong motivation to further our understanding of the interactions between trace metals, primary production, and carbon cycling in Fe-deficient systems like the Southern Ocean. Given very low external supplies of dissolved Fe (dFe; operationally defined with 0.2 µm filter), the importance of Fe recycling in sustaining primary production on various scales in the ocean has become increasingly apparent[11–14]. Yet, the key mechanisms for recycling Fe in the ocean remain unclear.

Zooplankton and larger marine biota—including salps, krill, seabirds, and whales—have been implicated as important players in trace metal recycling[15–19]. Antarctic krill (*Euphausia superba*, hereafter 'krill') are seen as substantial, dynamic Fe reservoirs in the Southern Ocean[18,20], and Antarctic baleen whales dive to consume several tonnes of krill each day at peak feeding times[21], excreting large quantities of fecal material at the surface that is rich in macronutrients and trace metals known to limit primary productivity[22]. This process of moving and transforming nutrients, referred to as 'the whale pump'[23], is a key pathway in which whales act as marine ecosystem engineers[24].

[1]School of Oceanography, University of Washington, Seattle, WA, USA. [2]Astrobiology Program, University of Washington, Seattle, WA, USA. [3]Hopkins Marine Station, Stanford University, Pacific Grove, CA, USA. [4]National High Magnetic Field Laboratory, Florida State University, Tallahassee, FL, USA. [5]Department of Ocean Sciences and Institute for Marine Science, University of California Santa Cruz, Santa Cruz, CA, USA. [6]Cascadia Research Collective, Olympia, WA, USA. [7]Cooperative Institute for Climate, Ocean, and Ecosystem Studies, University of Washington, Seattle, WA, USA. [8]Pacific Marine Environmental Laboratory, National Oceanic and Atmospheric Administration, Seattle, WA, USA. ✉e-mail: pmonreal@uw.edu; rbundy@uw.edu

In the 20th century, 1.5 million baleen whales were slaughtered in the Southern Hemisphere, including >95% of the largest species—fin (*Balaenoptera physalus*) and blue whales (*B. musculus*)[25,26]. Contrary to expectations, krill biomass on the former whaling grounds declined sharply (>80%) in the decades following whaling, particularly in the Southern Ocean[27], and data on krill predators has not conclusively pointed to population expansions consistent with the 'krill surplus hypothesis'[28–31]. A proposed mechanism to explain this krill paradox is that whales exert a top-down control on phytoplankton primary production by remobilizing nutrients, specifically bioavailable Fe[21]. Thus, industrial whaling could have contributed to a decline in epipelagic productivity by diminishing the recycling of growth-limiting micronutrients in surface waters[30,32]. However, several climate change-induced trends, such as warming and sea ice decline, and the growing krill fishing industry in the Southern Ocean have also and will continue to impact krill spatiotemporal distribution and baleen whale recovery[30,33,34]. Disentangling these anthropogenic impacts to the Southern Ocean and the ecosystem engineering capability of baleen whales requires further interdisciplinary research. For example, with Cu as a necessary cofactor for the krill respiratory pigment hemocyanin[35], it remains untested whether whales also concentrate and recycle toxic levels of Cu to primary producers.

Several recent studies have confirmed that marine macrofauna excrement is several orders of magnitude higher in Fe and other macronutrients than bulk seawater[17,18,22,23,36–40]. One report specifically examined the size fractionation of Fe in whale excrement and found hundreds of nanomolar of dFe, hundreds-to-thousands of times higher than Southern Ocean seawater[41]. Another study[22] noted bioconcentration of Cu in krill tissue and whale feces when reporting bulk Cu values. However, the total concentrations of trace metals do not directly translate to accessibility by microorganisms for uptake[42–45]. The chemical speciation of trace metals egested by whales or other marine predators has not been evaluated and is crucial to understanding if Fe recycled by whales is stable and bioavailable and if toxic species of other metals such as Cu are also excreted. Elucidating the effect that whales, krill, and other animals have on supplying and recycling bioactive trace elements such as Fe and Cu requires more detailed studies of their physicochemical forms upon excretion[36,37,41,46–49].

Ligands, organic compounds that can bind to metals, dictate the bioavailability, stability, scavenging rate, and residence time of dissolved trace metals in seawater[50]. Over 99% of dFe and dissolved Cu (dCu) in the marine environment is complexed by organic ligands[50–52], ranging from polysaccharides[53] and humic-like substances[54] with weak and intermediate binding strengths to high-strength metallophores—siderophores for Fe and chalkophores for Cu[55–57]. From promoting dissolution of Fe from minerals[58] to detoxifying free Cu ion[59], microbially-produced metallophores serve an outsized role in complexation despite our narrow knowledge of their dynamics, making their quantification in environmental samples of particular interest. Although we know of over 700 unique siderophore compounds[60], less than 20 Cu-binding metallophores have been described in marine environments[52,56,61,62].

Organic ligand measurements have not been conducted on whale excrement but are useful for describing the bioavailability ('bioavailability' hereafter refers to the degree to which the Fe or Cu pool is available for utilization by the microbial community[42]) of recycled trace elements[42,50,63], which, in turn, can inform models of the biogeochemical impact of egesta on the surface ocean[46,48,49]. For example, the presence of siderophores, despite enhanced stability and residence time[64], generally decreases the bioavailability of the Fe pool to eukaryotic phytoplankton[63]. The siderophore ferrioxamine has even been shown to be ~1000 times less bioavailable than unbound inorganic dFe (free Fe or Fe′)[43]—widely accepted as the Fe species with the highest uptake rates[43,65]—and ~15 times less than the average seawater Fe-ligand pool[44]. Similarly, strongly-bound Cu complexes are much less accessible than unbound Cu^{2+}, making Cu^{2+} the most bioaccessible (and therefore potentially toxic) form of dCu[66]. Unlike metallophores, exopolysaccharides have been shown to significantly enhance the bioavailability of the Fe pool for all studied organisms[42,53]. In this way, the contributions of various Fe species in fecal material relative to seawater can be leveraged to assess micronutrient bioavailability in the dissolved phase. For the particulate phase, chemical leaches that describe the lability of elements have been employed in prior work to describe potential bioavailability[67,68].

We present the first chemical characterization of the Fe- and Cu-ligand pools in fecal matter from large marine predators, using trace metal, electrochemical, and mass spectrometric techniques on two humpback whale (*Megaptera novaeangliae*) fecal samples from the Southern Ocean and three blue whale (*Balaenoptera musculus*) fecal samples from the California Current. We focus the application of findings to the Southern Ocean, where hypotheses about the impact of megafauna on metal cycling have centered, but fecal samples from the Southern Ocean are exceedingly rare. Given this, samples from the more accessible California Current were also analyzed to provide additional data. Detailed chemical measurements of these excrement samples help resolve the plausibility of the 'whale pump' hypothesis[23,46] by illustrating the bioavailability of limiting micronutrients mobilized by a baleen whale during feeding—a process which consumes thousands of kilograms of krill from the filtration of millions to tens of millions of liters of seawater per individual every day[21]. More broadly, through the characterization of novel Cu-chelating compounds, these data also illuminate how micronutrients are altered as they undergo marine mammal gastrointenstinal processes, with relevance to ecosystem-level trace metal cycling[47].

Results

Fecal iron-ligand pool suggests high iron bioavailability

In general, whale fecal samples exhibited large ranges in trace metal and ligand concentrations, consistent with the heterogeneity of fecal material and unavoidable mixing of background seawater prior to sampling[41]. Treating the excrement as seawater samples to allow for direct comparison with published values, we found high dFe concentrations in our samples. While one blue whale sample from the California Current (sample MSS1) contained 12.6 μM dFe (Fig. 1A, Supplementary Table 1), the [dFe] in the four other samples (238 nM–1.23 μM) aligned well with the only other set of dFe measurements in whale excrement (186–754 nM)[41]. A seawater sample collected alongside sample MN19 from the Southern Ocean was below detection for dFe using the method employed for the fecal dFe (see methods for additional details), demonstrating that contamination was negligible given high dFe concentrations in fecal samples. With typical sub-nanomolar surface concentrations of dFe in the Southern Ocean and California Current system[69–71], the dissolved fraction of baleen fecal samples was between 10^3 to over 10^5 times higher than average [dFe] in the open ocean.

Consistent with the high water-soluble organic carbon concentrations that have been reported in excrement[39], organic ligand analyses via competitive ligand exchange adsorptive cathodic stripping voltammetry (CLE-ACSV) titrations[72] yielded an enormous weakly-binding organic Fe-ligand pool in all of the samples. The total organic Fe-binding ligand concentrations ($[L_{Fe}]_{CSV}$) ranged from 100–645 μM eq Fe (reported as binding equivalents[50]), and the binding strengths (log $K^{cond}_{FeL,Fe'}$; conditional stability constant[50]) of the most abundant ligands ranged from 8.20–9.65, operationally placing them in the weakest ligand class (L_4) for seawater (Fig. 1B, E; Supplementary Tables 1–2)[50,73]. The best-fit complexation models for each sample also included a pool of intermediate-strength L_2 ligands, with average log $K^{cond}_{FeL_2,Fe'}$ = 11.57. These ligands made up 20% of reported $[L_{Fe}]_{CSV}$ values for MSS1 and between 0.5–3% of $[L_{Fe}]_{CSV}$ for the other four samples (Fig. 1B, E; Supplementary Tables 1–2). These values are quantitative, but were at the edge of the detection window, so have larger uncertainties (Supplementary Tables 1–2)[72]. While our dFe measurements agree with previously-published elevated Fe contents of baleen whale excrement in both the particulate[18,22] and dissolved phase[41], these are the first measurements of organically-complexed Fe in whale fecal material.

Similar to the [dFe], all baleen whale samples contained orders-of-magnitude greater dFe-binding ligand concentrations than the surrounding seawater, and all had much higher L_{Fe} than dFe. Concentrations of L_{Fe} in the

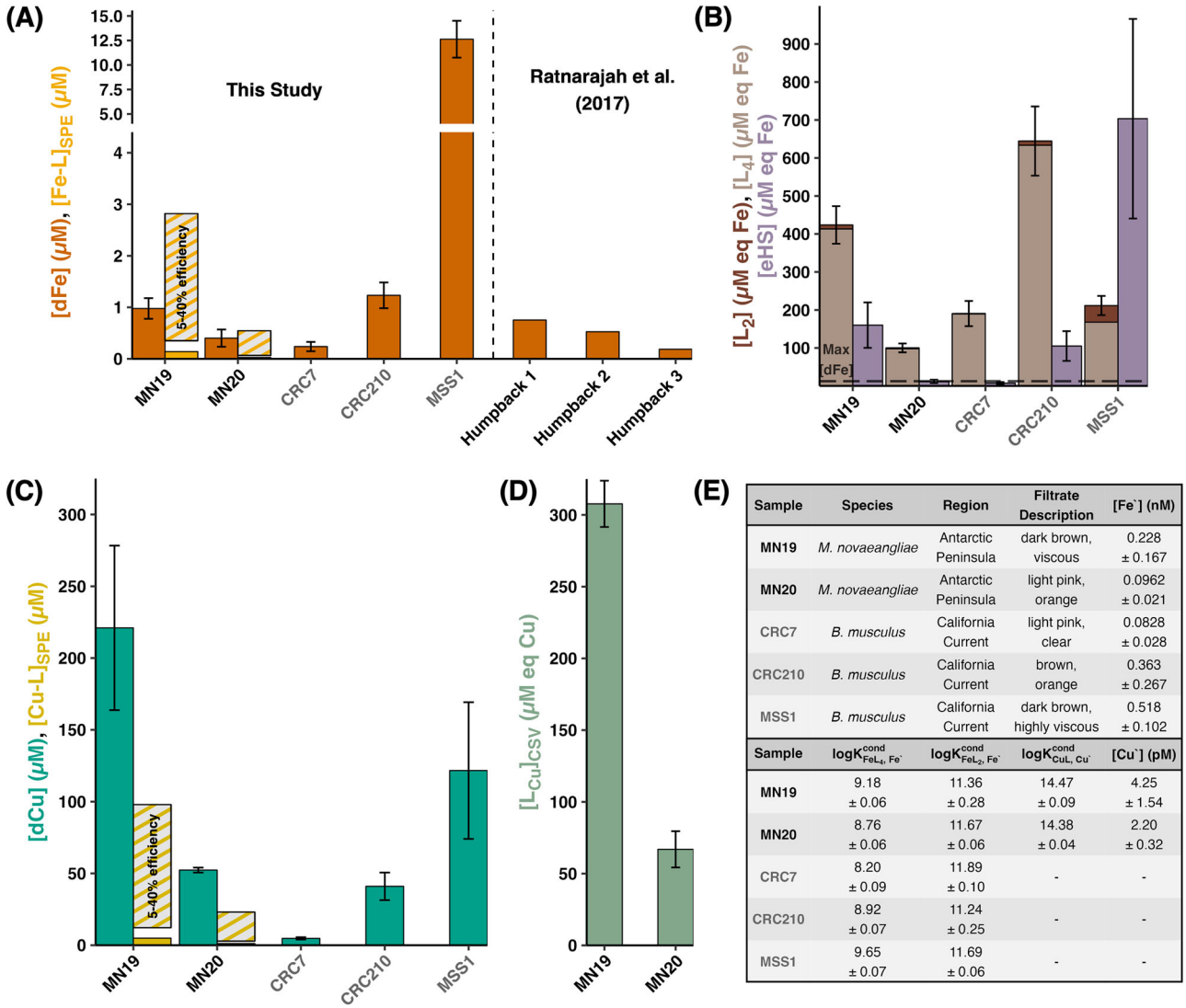

(E)

Sample	Species	Region	Filtrate Description	[Fe`] (nM)
MN19	*M. novaeangliae*	Antarctic Peninsula	dark brown, viscous	0.228 ± 0.167
MN20	*M. novaeangliae*	Antarctic Peninsula	light pink, orange	0.0962 ± 0.021
CRC7	*B. musculus*	California Current	light pink, clear	0.0828 ± 0.028
CRC210	*B. musculus*	California Current	brown, orange	0.363 ± 0.267
MSS1	*B. musculus*	California Current	dark brown, highly viscous	0.518 ± 0.102

Sample	$\log K^{cond}_{FeL_4, Fe'}$	$\log K^{cond}_{FeL_2, Fe'}$	$\log K^{cond}_{CuL, Cu'}$	[Cu`] (pM)
MN19	9.18 ± 0.06	11.36 ± 0.28	14.47 ± 0.09	4.25 ± 1.54
MN20	8.76 ± 0.06	11.67 ± 0.06	14.38 ± 0.04	2.20 ± 0.32
CRC7	8.20 ± 0.09	11.89 ± 0.10	-	-
CRC210	8.92 ± 0.07	11.24 ± 0.25	-	-
MSS1	9.65 ± 0.07	11.69 ± 0.06	-	-

Fig. 1 | Dissolved iron, copper, and metal-binding ligand concentrations. **A** Dissolved iron concentrations ([dFe]) of our sample set compared with the only other published [dFe] from whale feces[41], along with the solid-phase extracted concentration of ligand-bound iron ($[Fe\text{-}L]_{SPE}$) from LC-ICP-MS for samples MN19 and MN20. The striped bar represents the predicted concentration range of metal-binding ligands assuming a 5–40% extraction efficiency. **B** Ligand concentrations of the two Fe-binding ligand pools ($[L_2]_{CSV}$ and $[L_4]_{CSV}$) determined with competitive ligand exchange adsorptive cathodic stripping voltammetry (CLE-ACSV), and Fe equivalents for electroactive humic-like substance concentrations ([eHS]) calculated using 23.3 nM Fe per mg/L, the midpoint of the estimated binding envelope of humic and fulvic acids[101]. A horizontal line representing the highest [dFe] value of our samples is added to emphasize how large the ligand pool was relative to [dFe]. **C**–**D** Equivalent data but for copper species. **E** Table with conditional stability constants and free metal concentrations from CLE-ACSV and additional descriptions of the fecal samples. Error bars for the trace metal concentrations represent 1.96 standard errors between two inductively coupled plasma mass spectrometry (ICP-MS) runs with three replicate measurements per run, error bars for ligand data represent standard error determined with ProMCC[115], and error bars for [eHS] represent the full estimated binding envelope of humic and fulvic acids (14.6–32 nM Fe per mg/L). Labels for Southern Ocean and California Current samples are black and gray, respectively. Photo of filtered sample provided in Supplementary Fig. 4.

open ocean south of 50°S range from 0.04–15.7 nM eq Fe with typical log $K^{cond}_{FeL,Fe'}$ from ~10–12.4[45,74]. A study from the Southern California Current using multiple analytical windows measured ~1–3 nM eq Fe of ligand classes L_{1-3}, but no class with log $K^{cond}_{FeL,Fe'} < 10$ was detected[75]. Little is known about the identity of these weak L_4 ligands, but they likely represent simpler, weakly-binding organics and degradation products[75]. Despite hundreds of μM eq Fe of ligands in excess of dFe, the overall weak strength of the Fe ligand pool allowed for relatively high concentrations of calculated free Fe ([Fe′] = 83–518 pM; Fig. 1E; Supplementary Table 1). Given typical [Fe′]< 1 pM in the open ocean[76], we expect high bioavailability and fast uptake rates of dFe excreted by whales.

We leveraged liquid chromatography coupled to inductively coupled plasma mass spectrometry (LC-ICP-MS) and electrospray ionization mass spectrometry (LC-ESI-MS) to further probe the structural features of these ligand pools and better understand the fate of recycled Fe and Cu. Following a solid-phase extraction and elution step, we can detect metal-bound organic compounds using LC-ICP-MS, and using the same LC protocol, LC-ESI-MS provides the exact mass of putative metal-bound compounds[55–57,77]. The LC-ICP-MS ^{56}Fe chromatogram exhibited a large, heterogenous mix of ligands eluting toward the start of the solvent gradient, where more polar species elute, with two minor humps eluting in the less-polar section of the gradient (Supplementary Fig. 1). However, no large discrete peaks were detected, indicating that individual ligands such as siderophores were too low to detect or obscured by the large pool of chromatographically-unresolved ligands. Additionally, due to high-Fe content and volume constraints, only 3–10 mL of sample were used, whereas similar analyses with seawater have used 4 L or more of sample[55–57,77].

The broad peak of chromatographically-unresolved ligands (Supplementary Fig. 1), combined with a feature on the voltammograms at E ~ -0.6 V (Supplementary Fig. 2), suggested that humic-like substances may be important components of the ligand pool. Humic-like ligands refer to a heterogenous class of compounds with carboxylic acid, phenolic, and/or N- and S-containing functional groups that complex Fe with intermediate binding strength[78,79]. The feature at E ~ -0.6 V increased upon standard addition of Suwannee River Humic Acid to our samples[80], confirming a high concentration of electroactive humic-like substances (eHS; Supplementary Fig. 3), ranging from 4.72 μM eq Fe to over our largest $[L_{Fe}]_{CSV}$ value of 644.6 μM eq Fe. Exopolymeric substances (EPS) may also be detected by the humic standard addition method[53], meaning that EPS, humic-like compounds, or a combination of both were likely the intermediate L_2 class of ligands detected in these samples.

Large fecal dissolved copper pool is tightly complexed by novel metallophores

Despite reported bioconcentration of Cu in krill tissue and whale fecal matter[22], there are no published values for fecal dCu in the literature, making it impossible to determine if whales recycle free copper (Cu′) above toxicity thresholds for phytoplankton. We characterized the dCu pool with similar methods used for the dFe pool and found extremely high levels of dCu (4.54–198 μM; Fig. 1C; Supplementary Table 1) relative to seawater[71]. The Cu-based oxygen-transport proteins in krill hemolymph[35] help explain the elevated dCu levels in our samples. Due to sample volume limitations, we were only able to quantify the Cu-binding ligand concentration ($[L_{Cu}]_{CSV}$) in the two Southern Ocean samples. While $[L_{Cu}]_{CSV}$ for samples MN19 and MN20 (307.7 and 66.93 μM eq Cu, respectively; Fig. 1D; Supplementary Table 1) was of similar magnitude to $[L_{Fe}]_{CSV}$, the Cu-binding ligands were orders-of-magnitude stronger than the Fe-binding ligands, with $\log K^{cond}_{CuL,Cu'} = 14.38$ and 14.47—on the high end of previously-reported values for seawater (Fig. 1E; Supplementary Table 1)[52].

Cu-binding ligands are typically stronger than the Fe-ligand pool[81], possibly reflecting the production of strong Cu metallophores (chalkophores) to detoxify Cu^{2+} in the marine environment[59]. One study[66] has demonstrated that tightly-complexed dCu may be accessed via cell surface reductases and thus remains somewhat bioavailable to surface phytoplankton, suggesting the dCu pool in this study could still be utilized as a micronutrient if needed, albeit at lower rates than dFe. We calculated free Cu ([Cu′]) of only 3–4 pM in the whale fecal samples, indicating that the strong Cu ligands present in whale excrement maintained [Cu′] below the 10^{-11} M toxicity threshold cited for most marine phytoplankton[7,82], despite the micromolar amounts of dCu in the samples (Fig. 1E).

The Cu-binding ligand pool that we observed using LC-ICP-MS contained a similar broad feature as that of the ^{56}Fe chromatogram (Supplementary Fig. 1) at the start of the mobile phase (Fig. 2A), implicating humics or EPS as relevant ligands for Cu as well. Starkly contrasting with Fe, however, the Cu chromatogram was dominated by several large, discrete peaks (Fig. 2A), implying the presence of distinct chalkophores in the samples, which is in line with the high average values for $\log K^{cond}_{CuL,Cu'}$ (Fig. 1E). Little is known about the behavior of chalkophores in the marine environment, with few compounds described to date[52,56,61,62]. Recent work has proposed putative Cu ligands as structures with high degrees of unsaturation and N- or S-containing functional groups, namely linear tetrapyrroles[61] or azole-containing compounds[56].

In sample MN19 alone, nearly 50 unique masses were identified as putative Cu-containing compounds (Fig. 2A, Supplementary Table 3), more than doubling the number of known Cu metallophores from marine samples[52,56,61,62]. These putative compounds were confirmed with two corresponding LC-ESI-MS peaks with a change in mass-to-charge ratio equal to the mass difference of ^{63}Cu and ^{65}Cu and intensity ratios equal to the natural abundance ratio of ^{63}Cu/^{65}Cu (Fig. 2)[56,61,62,77]. We further characterized these compounds by obtaining putative molecular formulae for 37 of the Cu metallophores (Supplementary Table 3–4), leveraging highly-accurate exact masses from the 21 Tesla Fourier transform ion cyclotron resonance mass spectrometer (FT-ICR-MS, see methods for additional details)[83,84].

The apo (without metal) versions of the 37 assigned formulae in Supplementary Table 3 have an average molecular ratios of H/C = 1.29 ± 0.09 (± 1 SD), O/C = 0.20 ± 0.03, and N/C = 0.13 ± 0.03. The elemental compositions cluster in van Krevelen space (Fig. 3) with known linear tetrapyrroles in biology and are very close to a recent characterization of tri- and tetrapyrrolic Cu ligands in diatom cultures (Fig. 3), but with slightly higher H/C ratios[62]. The chromatography employed in that work[62] indicates that the ligands were also of similar polarity to those described here. Also similar to prior work[61], our chromatograms contained multiple metal-bound peaks with the same exact mass (Supplementary Fig. 5), suggesting isomers are common. One putative Cu ligand in this study ($m/z = 664.196$) was detected previously in extract from an axenic *Synechococcus* culture, and fragmentation data (MS2) collected on the 21 T linear ion trap (Supplementary Fig. 6) revealed a shared abundant fragment with that prior work[61]. Furthermore, MS2 spectra collected for at least five of the putative Cu ligands exhibit loss of putative terminal pyrrole groups (Supplementary Fig. 6), which has been observed during fragmentation of bile tetrapyrroles urobilin and stercobilin[85], and similar fragmentation was observed in seawater Cu ligands[61,62]. These lines of evidence suggest that many of the strong Cu ligands in the fecal samples are tetrapyrroles.

Whales excrete highly-labile particulate metals

Although we were primarily focused on the dissolved phase, we also sought to characterize the lability of the particulate fraction of whale excrement. Particulate Fe (pFe; >0.2 μm) concentrations ranged from 5–22.5 μM in the previous physical speciation analysis[41], which is comparable to some dFe levels found in this study. A 25% v:v acetic acid and 0.02 M hydroxylamine hydrochloride leach with a short heating step (i.e., Berger leach) has been used in previous work to operationally represent the fraction of particulate metal that can be accessed by grazing, photochemistry, redox processes, and ligand-associated dissolution on the same timescale as phytoplankton generations (days)[67]. Using this weak chemical leach, the labile particulate Fe ($[pFe]_{labile}$) for samples MN19 and MN20 was 1.41 and 0.75 mmol Fe kg^{-1} dry weight, and $[pCu]_{labile}$ was 1.82 and 2.72 mmol Cu kg^{-1} dry weight, respectively (Fig. 4; Supplementary Table 1). Remarkably, this lability leach recovered concentrations close to the total Fe and Cu contents of baleen whale fecal samples determined via nitric acid digestion in prior reports[18,22] (Fig. 4), implying that a large proportion of pFe and pCu in fecal samples is labile.

Comparing results from our Berger leaches to the lowest and highest [pFe] values from nitric acid digestion[18], pygmy blue (*B. m. brevicauda*) and fin (*B. physalus*) whales, respectively, yields a large lability range (17.6–100%) that highlights the high variability of these types of samples. Since samples MN19 and MN20 are humpback whale samples, specifically using the mean and standard deviation for humpbacks reported in that study[18] yields a tighter window of 28.1–89.0% lability for pFe. This is in contrast to other sources of pFe to the ocean such as dust, which are often assumed in models to have 1–10% lability[86]. Of course, fecal samples are heterogenous and these are separate samples; while it is possible that our two humpback whale samples had very different total Fe and Cu than those from previous analyses[18,22], the Fe:P ratios from our weak leaches and the Fe:P ratios of total digestions in that study are also comparable (Fig. 4), along with the dFe[41] (Fig. 1A), indicating that physicochemical parameters like biogenicity, size fractionation, and metal-ligand content are reasonably similar. Taken together, this suggests that the particulate phase of cetacean fecal matter is highly labile, likely due to the high organic content.

Discussion

Our analyses assessed the chemical speciation and potential bioavailability of trace metals recycled by baleen whales via characterization of excreted ligands. Although whales excrete unprecedented levels of dCu, the strong-binding nature of excreted ligands maintains [Cu′]—the most toxic species

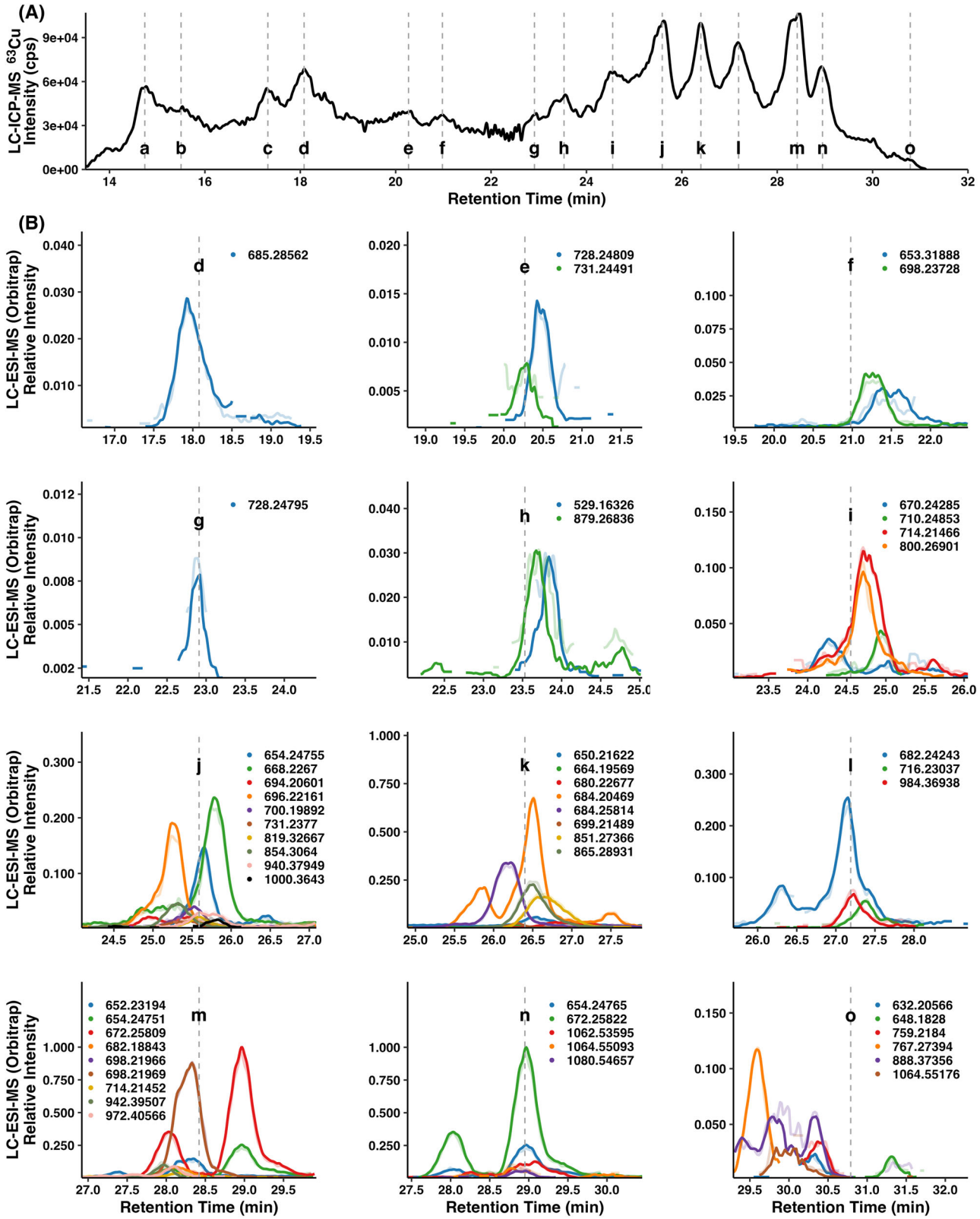

—below toxicity thresholds. Our most unexpected outcome was the identification of novel Cu-binding metallophores in the fecal excrement. We have limited knowledge about the nature of chalkophores in the marine environment, since <20 total chalkophores have been identified so far[52,56,61,62]. By comparison, we found nearly 50 new candidate masses that strongly bind to Cu based on LC-ICP-MS and LC-ESI-MS data in only one sample of whale excrement. These compounds comprised peaks in the LC-ICP-MS chromatogram that conservatively represent 471 nM Cu (assuming 100% extraction efficiency and only integrating area above chromatogram baseline; Fig. 2, Supplementary Table 2). In-depth and definitive structural characterization was outside the scope of this project, but our putative assignments provide candidates for future analyses that will further

Fig. 2 | Mass spectra for copper-binding compounds in sample MN19. A Copper-63 (^{63}Cu) chromatogram from liquid chromatography-inductively coupled plasma mass spectrometry (LC-ICP-MS) analysis, with dashed lines denoting peaks or areas that were parsed for Cu-binding masses with liquid chromatography-electrospray ionization mass spectrometry (LC-ESI-MS) data. **B** Extracted ion chromatograms (EICs) of Cu-binding compounds identified with LC-ESI-MS, binned into retention time windows corresponding to peaks d–o of (A) (EICs for peaks a–c not plotted). The y-axes for (**B**) are LC-ESI-MS intensities relative to the candidate mass-to-charge ratio with the highest intensity (m/z = 672.258). Candidates were identified by two corresponding ESI-MS peaks with $\Delta m/z$ = 1.9982 and intensity ratios equal to the natural abundance ratio of ^{63}Cu/^{65}Cu. Solid-colored EICs represent the mass of the ^{63}Cu-bound isotopologues, while transparent-colored EICs represent the ^{65}Cu-bound isotopologues, multiplied by 2.2 according to the natural abundance ratio of ^{63}Cu/^{65}Cu. Thus, agreement between solid and corresponding transparent lines provide evidence that candidate is a Cu-containing compound. The legend lists the exact masses of the ^{63}Cu-bound EIC peaks, as obtained from Fourier transform ion cyclotron resonance mass spectrometry (FT-ICR MS) data. More information about these peaks given in Tables S3–S4.

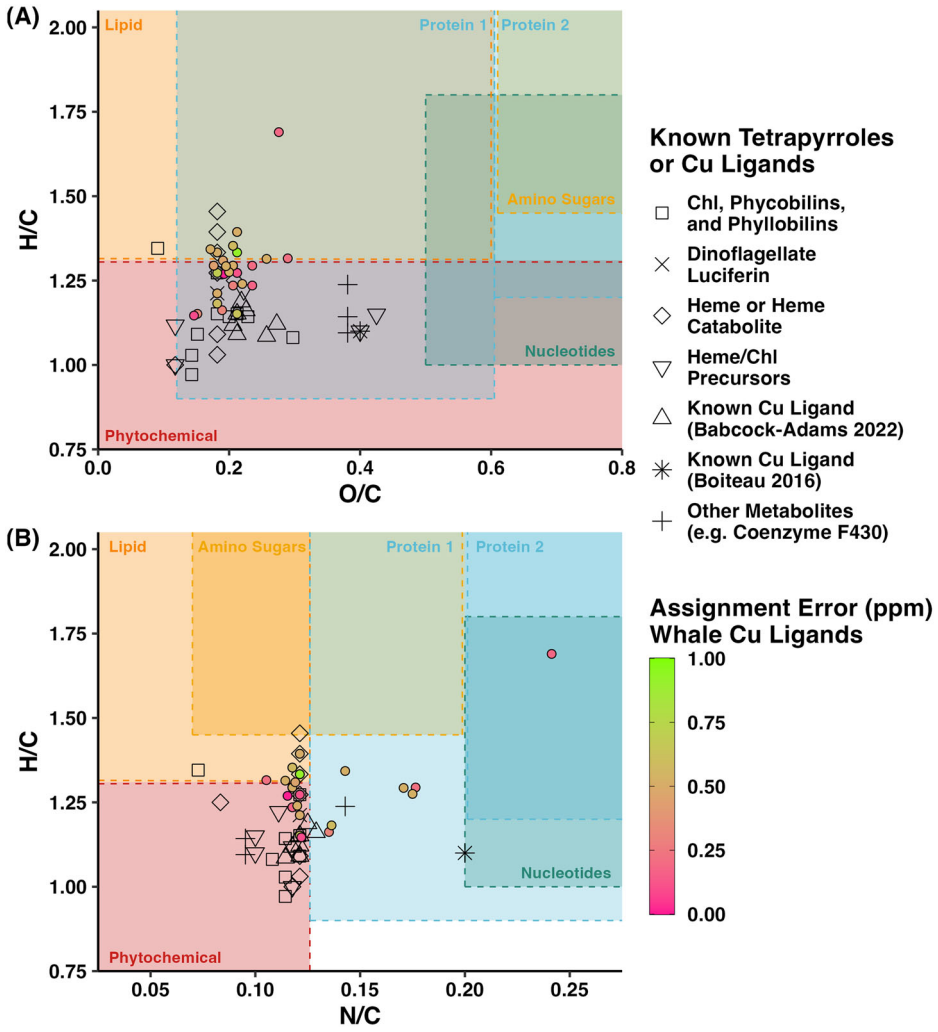

Fig. 3 | Van Krevelen diagrams of fecal copper ligands and known tetrapyrroles. A Elemental ratios (H/C versus O/C) and **B** H/C versus N/C of the apo (without metal) structures of copper (Cu) ligands in this study with assigned molecular formulae are plotted with colored points, while other symbols represent known tetrapyrroles or previously-characterized Cu ligands from marine samples[56,61]. The colors of the points represent the assignment error between the observed m/z and the monoisotopic mass of the assigned formulae. Recent multidimensional stoichiometric compound classification (MSCC) constraints are denoted by shaded regions, although it should be noted these constraints also include phosphorous ratios, mass, and number of atoms in the complete classification scheme[119].

advance our understanding of Cu biogeochemistry in the marine environment.

The fecal metallophores share formulae or cluster stoichiometrically (Fig. 3) with known linear tetrapyrroles. For example, apo ligand $[C_{33}H_{41}N_4O_6]^+$ matches that of ionized dinoflagellate luciferin (responsible for bioluminescence)[87] and cyanobacterial pigment phyocyanobilin. Particularly apt for fecal samples, highly-abundant $[C_{33}H_{43}N_4O_6]^+$ and $[C_{33}H_{45}N_4O_6]^+$ match formulae of bile pigment urobilin and precursor urobilinogen[88], respectively (structures in Supplementary Fig. 7), and MS-MS spectra show loss of terminal pyrrole groups (Supplementary Fig. 6) similar to prior work with bile tetrapyrroles[85]. One of the largest peaks, $[C_{33}H_{41}O_6N_4SCu]^+$, appears related to other ligands simply by addition of a sulfur functional group, which can occur through cysteine-related pathways[89]. In this way, a majority of the novel Cu chelators in the excrement appear to be directly related to heme or chlorophyll catabolites, such as bile pigments[88], phyllobilins[90], and even dinoflagellate and krill luciferins[87]—some of which have been demonstrated to form complexes with Cu[91].

While there is one shared formula and general similarities with previously-characterized seawater Cu ligands, the stoichiometric ratios of the Cu ligands in this study—driven by elevated H/C ratios—cluster separately from those previous studies[56,61] (Fig. 3), indicating distinct but related ligands in fecal samples. Considering stoichiometric similarities with bile pigments (Fig. 3), these novel Cu ligands could be produced from heme-related metabolites within baleen whales by their gut microbiota in response to high Cu loads. On feeding days in the Antarctic, humpback whale can consume an estimated 3 tons d^{-1} [21]. Combined with the Cu content of whole krill (98 mg kg^{-1})[22], this prey consumption rate translates to nearly five moles of Cu entering the gastrointenstinal system each day of Antarctic feeding, highlighting a need for strong Cu-chelating metabolites. Another plausible source of chelators is the breakdown of krill proteins, as their oxygen-transport proteins use Cu. A third option, similar to heme or chlorophyll catabolites, are ligands with a corrin ring like vitamin B_{12}, but the molecular signature of the most-abundant ligands are more similar to heme

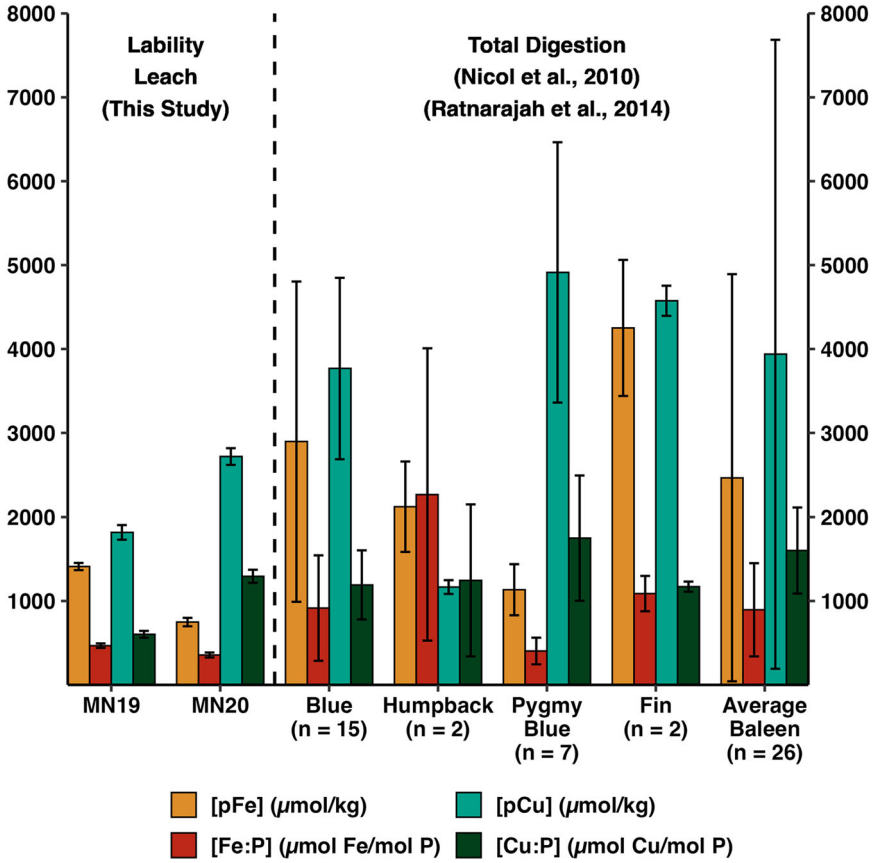

Fig. 4 | Lability leach results of MN19 and MN20 compared to published bulk particulate data. Berger leaches were conducted on humpback fecal samples MN19 and MN20 to quantify the labile particulate iron ($[pFe]_{labile}$) and copper ($[pCu]_{labile}$) concentrations. Concentrations are plotted in μmol metal kg^{-1} dry weight and ratios are plotted in μmol metal mol^{-1} P to allow easier comparison with Fig. 1. Leach concentrations were similar in magnitude to literature values for bulk Fe and Cu content determined via nitric acid digestion[18,22]. Error bars for previously-published values were reported as one standard deviation of mean values for each species. Since the leaches in this study are presented as individual samples, error bars for MN19 and MN20 were derived from standard curve uncertainty.

catabolites rather than hemocyanin or vitamin B_{12}, and diving mammals contain elevated levels of hemoproteins[92].

The suggestion of linear tetrapyrroles as strong Cu chelators in seawater[61,62], specifically heme or chlorophyll catabolites, has large implications for Cu dynamics, as these are ubiquitous molecules utilized and cycled by every trophic level[93]. Indeed, several masses corresponding to the chalkophores in this study have been detected in preliminary analyses of seawater samples from the Western Antarctic Peninsula[94]. This study posits gut flora as likely producers of these chalkophores, either by transforming heme-related compounds in the whale gut, cyanobacterial pigments moving through the food chain, or krill proteins from baleen prey, but more metagenomic work is needed to further investigate these processes.

Little is currently known about the baleen whale gut microbiome, but one study[95] found a higher proportion of reads assigned to the dominant phyla Firmicutes relative to terrestrial mammals, and several Firmicutes genera were chitinolytic and found to be closely associated with krill exoskeletons in samples from the forestomach of common minke whales (*B. acutorostrata*)[96]. It has been proposed that the multichambered stomach of baleen whales may result in longer digestion times, higher numbers of bacteria, and therefore, more complete digestion of krill relative to other krill predators like seals and penguins[96]. Therefore, baleen whales (through their gut microbiome) may have an ability to convert prey into micronutrients more efficiently relative to other predators who filled that niche post-whaling. More broadly, if the animal gut microbiome is transforming environmentally-relevant amounts of micronutrients, the role of these living bioreactors in local and regional biogeochemical cycling needs to be further considered.

The egested Fe-ligand pool, dominated by weakly-binding (L_4) ligands with considerable concentrations of EPS- or humic-like ligands (L_2), greatly contrasted with the Cu-ligand pool. We have limited knowledge of the fate and dynamics of L_4 ligands[73]. Interestingly, domoic acid—a neurotoxin produced by diatoms—has a binding strength ($\log K^{cond}_{FeL,Fe'} = 8.7 \pm 0.5$)[97] that is remarkably similar to that of the L_4 pool detected here, bioaccumulates up the food chain, and has previously been detected in whale feces[98]. It also plays an important role in Cu-dependent, high-affinity Fe acquisition systems of diatoms[99], making domoic acid an intriguing potential Fe-ligand excreted by whales. However, its hydrophilic nature could cause poor retention in the solid-phase extraction method employed for siderophores, and its ions were not found in our data (Supplementary Fig. 8).

While speciation parameters cannot quantitatively predict Fe uptake rates[44,45], prior work has demonstrated certain ligand species to either enhance or decrease the overall bioavailability of dFe in the marine environment[42,53,63,65]. For example, Fe′ is considered the most bioavailable Fe species[43], with variations in [Fe′] explaining significant variations in phytoplankton Fe uptake in a recent experiment in the Southern Ocean[65]. Additionally, algal exudates of large polysaccharides are known to complex Fe with intermediate strength[100] and greatly enhance Fe bioavailability in seawater[42,53]. In this study, we quantified marine-derived humic-like substances, which have been found associated with dFe in several ocean basins[101] and may allow for distal transport of dFe[102], but the relationship between [eHS] and bioavailability is not immediately clear[45]. That said, the fact that EPS may also be detected by standard addition of humics[53], the mucosal nature of excrement samples, and the putative role of gut microbiota are all consistent with exopolymeric substances as the L_2 ligands in these samples.

Contextualizing our datasets with previous bioavailability studies, a picture of a highly-bioavailable dFe pool emerges. Upon defecation, micromolar levels of dFe are released into seawater in a loosely-bound organic matrix, yielding ~0.1–0.5 nM of extremely bioavailable Fe′—10^3–10^5 times higher than typical surface seawater values[76]. The lability of Fe′ and lack of dFe in HNLC waters may enable rapid uptake of excreted dFe by the microbial community. Speciation calculations (Supplementary Table 2) predict that most of the complexed dFe is preferentially bound to the intermediate-strength L_2 ligands when released in seawater. While less abundant than the weaker L_4 ligands, their strength and relative abundance allow them to outcompete the weaker degradation products and to stabilize

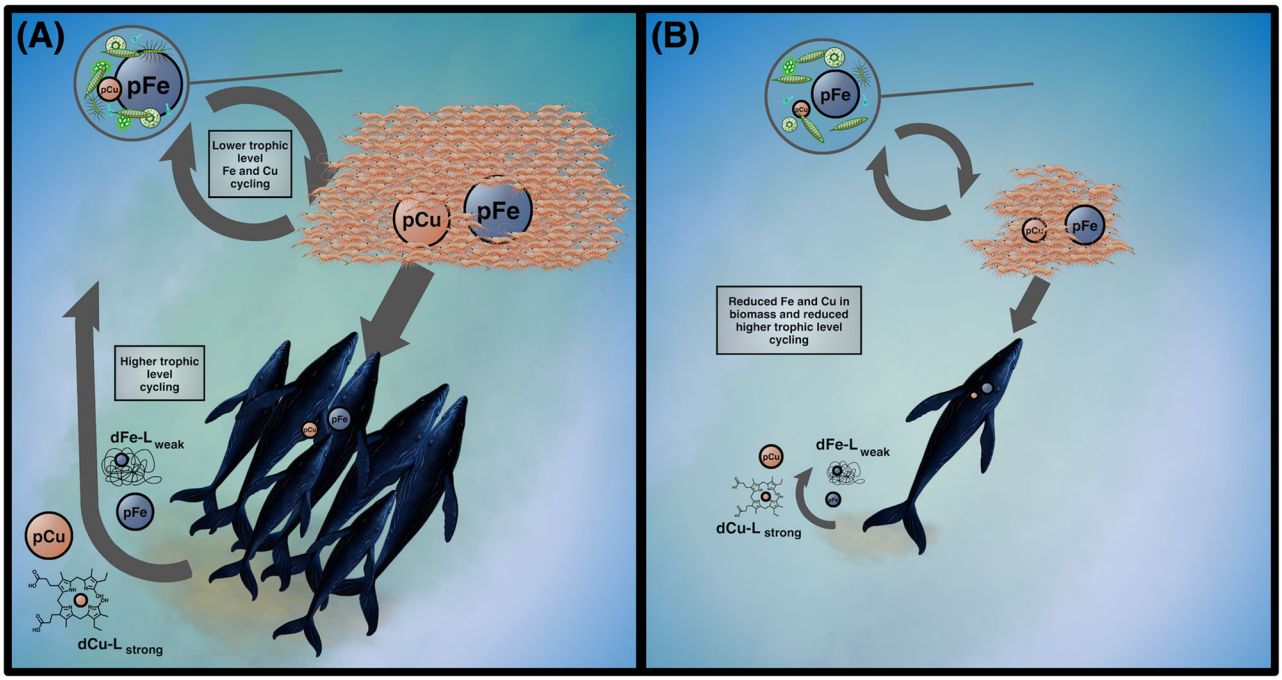

Fig. 5 | Disruption of iron and copper recycling from industrial whaling. A depiction of the (**A**) pre-whaling and (**B**) post-whaling phytoplankton-krill-whale interactions in the Southern Ocean. The decimation of whales in this ecosystem and sharp decline in krill biomass in some former whaling grounds imply a large shift in biogenic pFe due to biomass changes alone.

the dFe pool, preventing precipitation and loss from surface waters. Since seawater does not have sufficient unbound ligands for binding the high amounts of dFe excreted by whales, the fact that this dFe is already organically-complexed is crucial for ensuring this Fe is not immediately lost from solution. Furthermore, the putative EPS-like characteristics of the L_2 pool imply enhanced bioavailability for the eukaryotic phytoplankton[42,53] of the Southern Ocean. Thus, the Fe-binding ligand pool in our samples suggest that baleen whales supply immediately-bioavailable dFe that should remain relatively stable on longer timescales, lending support to hypotheses that whales provide important ecosystem services through recycling micronutrients within the epipelagic.

Not only do baleen whales—together with their gut microbiome—transform krill biomass into bioavailable dFe (Fig. 5), but the leaches confirm that the particles in excrement contain highly-labile pFe. Additionally, with excess ligands in the samples at hundreds of μM eq Fe, the sheer amount of excreted ligands may influence the Fe biogeochemistry of surrounding waters. Ligand-complexing capacity is thought to dictate Fe solubility, so it is possible that this injection of ligands itself could promote dissolution or the stabilization of other ambient Fe or additional labile pFe from the excrement[103,104]. Future work could investigate the impact of the fecal ligand pool on the ambient dFe pool using incubations or measure the uptake of fecal Fe in cultures. Doing so would provide the opportunity to test this bioavailability assessment derived from ligand characterization with other methods of defining bioavailability found in recent studies[44,45].

A recent report[21] measuring whale feeding behaviors and krill swarms estimated that the pre-whaling Antarctic minke (*B. bonaerensis*), humpback, fin, and blue whales in the Southern Ocean could have recycled between 1.25 and 2.69×10^8 mol Fe yr^{-1}. From a biogeochemical perspective, skepticism of the impact and utilization of nutrients recycled by marine megafauna lie, in part, around uncertainties in nutrient bioavailability and stability in the euphotic zone. We find that a large portion (28.1–89.0%) of the pFe fraction in baleen whale feces is operationally labile—consistent with the organic-rich and high-ligand content of egesta. For context, estimates of the total bioavailable Fe flux from ice melt, glacial sediment sources, and aeolian dust dissolution to the Southern Ocean today—also derived from leach data—are $1.79–8.95 \times 10^7$ mol Fe yr^{-1}, $1.07–2.15 \times 10^9$ mol Fe yr^{-1}, and $1.79 \times 10^8–2.33 \times 10^9$ mol Fe yr^{-1}, respectively[68]. Applying our findings to the estimate based on feeding behavior[21] suggests pre-whaling baleen populations could have recycled $3.51 \times 10^7–2.39 \times 10^8$ mol yr^{-1} of potentially-bioavailable Fe. If the recycled Fe persists in the photic zone long enough to be accessed and utilized by primary producers, whales may have regenerated a substantial amount of bioavailable Fe in the Southern Ocean (Fig. 5), which may have otherwise been lost through sinking krill biomass.

Modelling efforts to quantify the ecological and biogeochemical effect of whaling have often considered the entire area of the Southern Ocean, presenting a broad, basin-scale picture[29,48,49]. Conversely, tracking and ship-based survey data illustrate persistent foraging grounds that align with highly-productive waters for at least some Southern Ocean baleen whale populations[105–107]. Recent papers regarding upwelled Fe sources to large Southern Ocean phytoplankton blooms[108,109], in fact, have used whale activity as indicators of the enhanced productivity and overall strong ecosystems of their study areas[105,108–110]. These reports demonstrate that dense blooms, which support krill populations, are integral to the biogeography of baleen whale foraging in the Southern Ocean. While there can be a temporal offset between the initiation of diatom blooms and whale foraging, considering this spatial component, Fe recycling by baleen whales may be a highly-efficient process, whereby whales inject Fe-rich fecal plumes directly where high rates of primary production are occurring and where micronutrients may be most useful to sustain phytoplankton blooms[47] (Fig. 5).

During the 20th century, whalers harvested two million great whales (including half a million sperm whales) in the Southern Ocean[25,26], diminishing their recycling of total Fe by 90% (Fig. 5). It was previously unknown to what degree recycled Fe was bioavailable to phytoplankton—a critical unknown to the hypotheses surrounding the krill paradox and Fe recycling by whales[46]. Our results confirm that this Fe was highly labile. Furthermore, considering biomass changes alone, biogenic Fe reservoirs in phytoplankton, zooplankton, and macrofauna prior to the 20th century were much higher than in the modern Southern Ocean (Fig. 5)[49]. Taken together with the new empirical prey consumption rate calculations for baleen whales[21], Fe recycling between trophic levels was

likely even stronger than previously estimated (Fig. 5)[21,49]. The removal of whales from the Southern Ocean ecosystem, contextualized with the bioavailability characterization in this study, alludes to a pre-whaling ecosystem and associated Fe and carbon biogeochemistries that starkly differ from the boom-and-bust diatom blooms of today[111]. While some baleen whale populations have started recovering in the Southern Ocean, climate change-induced warming[33,112] and the expansion of krill fisheries[34] imperils krill numbers and whale recovery and, thus, will likely obscure biogeochemical impacts of population recovery. Although we focus implications on the Southern Ocean, samples from the California Current exhibited similar biogeochemistry, and the impact of large animals on nutrient limitation and ecology should be considered elsewhere. Finally, we found evidence of nearly 50 novel chalkophores in the recycled Cu pool that relieve organisms from toxic levels of the free Cu ion. A fraction of the strong Cu ligands described here are likely produced by the gut microbiome, which suggests that the microbiome modulates the speciation of recycled micronutrients—a hypothesis that could extend to a much wider range of animals. More interdisciplinary research across scales is needed to further unravel these biogeochemical facets of ecological mutualisms in the ocean.

Methods

Sampling and sample processing

Opportunistic samples of clumped whale excrement were collected floating on the surface near foraging whales using an aquarium mesh net. Samples MN19 and MN20 (abbreviated from "Mn19_031E_P" and "Mn20_062C_P") were collected from humpback whales (*Megaptera novaeangliae*) in nearshore waters along the western side of the Antarctic Peninsula. Samples CRC7, CRC210, and MSS1 (abbreviated from "CRC sighting #7", "CRC 20180829-210", and "MSS1") were collected from blue whales (*Balaenoptera musculus*) off the California coast. Maps of approximate locations of collections are provided in the supplement (Supplementary Fig. 9). Samples were separated from water as possible in the field, stored in sterile glass jars, and kept frozen at -20 °C until analysis.

Although sampling was not conducted under current trace-metal clean sampling procedures, the effect of contamination was likely minimal relative to typical metal concentrations of fecal matter. A seawater sample collected alongside sample MN19 allowed us to gauge how contamination-prone fecal collection was. Considering this as a sampling blank, this seawater sample was prepared for ICP-MS analysis using the same methodology as for the fecal samples (30-fold v:v dilution in 2% nitric acid, see below) and its signal intensity was similar to that of the ICP-MS blank, demonstrating that contamination during sampling was negligible. Since samples were primarily taken for ecological research, background seawater chemistry samples were not available for the other fecal samples. However, the sampling strategy was similar for all fecal samples.

After sampling, standard GEOTRACES procedures for analyzing trace elements in seawater were followed at each stage of sample processing[113] to allow direct comparison with published values. All plastic labware was acid-washed for at least 1 week in a 10% v:v nitric acid (HNO_3; trace metal grade, Fisher Chemical) bath, followed by 1 week in a 10% v:v hydrochloric acid (HCl; trace metal grade, Fisher Chemical) bath. For dissolved analyses, samples were filtered through a 0.2 µm polycarbonate track-etch membrane filter (Pall Corporation) mounted on an acid-cleaned Teflon vacuum filtration rig (Savillex Corporation) in a HEPA-filtered laminar flow bench. Aliquots for dissolved trace metal analysis were immediately acidified with Optima-grade HCl (Fisher Chemical) and stored at room temperature at pH 1.8. Aliquots for voltammetric analysis were immediately frozen after filtration and stored at −20 °C. For the two Southern Ocean samples, we loaded 3–10 mL of filtrate onto 6-mL polystyrene divinyl benzene (Bond Elut ENV, Agilent Technologies) solid phase extraction (SPE) columns that had been activated with Optima-grade methanol (Fisher Scientific) and rinsed with Milli-Q (Sigma-Aldrich). Finally, subsamples of the two Southern Ocean samples were also freeze-dried for further chemical leaches of labile particulate metal measurements.

Dissolved trace metals

All five fecal samples were analyzed for dissolved iron (dFe) and copper (dCu) with ICP-MS on an iCAP RQ (Thermo Scientific), using a similar methodology to a previous fecal analysis[41]. Filtered samples were diluted 30-fold in 2% (v:v) Optima-grade nitric acid (Fisher Scientific) and spiked with 1 ppb indium and rhodium to account for analysis drift and sample matrix effects. Duplicate aliquots for each fecal sample were prepared in this way, as well as a third set spiked with multi-element standards (Spectrum Chemical) to monitor the recovery of metals of interest in the sample matrices. Final concentrations were calculated with an eight-point standard curve ($R^2 > 0.99$) ranging from 0 to 4000 nM dFe and dCu, prepared in a similar manner to the samples with low-trace metal surface seawater from the equatorial Pacific.

Error in concentration was derived from uncertainty of the standard curve, according to:

$$s_{[M]} = \frac{s_r}{|m|}\sqrt{\frac{1}{k}+\frac{1}{n}+\frac{(S_{samp}-\overline{S_{std}})^2}{m^2\sum_{i=1}^{n}([M]_{std_i}-\overline{[M]_{std}})^2}}$$

where $s_{[M]}$ is the standard deviation in analyte concentration, calculated from the standard deviation about the standard curve regression, s_r; the slope of the standard curve, m; the number of replicate measurements, k; the number of standards, n; the sample's average signal on ICP-MS, S_{samp}; the average signal of the standards, $\overline{S_{std}}$; and the concentrations of standards used in the analysis, $[M]_{std}$.

Labile particulate trace metals

A weak acid leach was applied to freeze-dried subsamples of the two Southern Ocean fecal samples to quantify the concentration of labile particulate Fe ($[pFe]_{labile}$) and Cu ($[pCu]_{labile}$)[67]. Briefly, samples were heated in 5 mL of leach solution consisting of 25% v:v acetic acid (Sigma-Aldrich) at pH 2 and 0.02 M hydroxylamine hydrochloride (Fisher Scientific) at 90 °C for 10 min, left at room temperature for 3 hr 50 min, centrifuged for 5 min, and syringe-filtered with an acid-cleaned 0.2-µm polyvinylidene fluoride filter (Fisher Scientific). Then, 5 mL of Milli-Q was added before another 5 min of centrifugation and syringe-filtration. Finally, the filtrate was evaporated overnight at 130 °C, and the crystal residue was prepared for ICP-MS analysis and quantification as described above for the dissolved trace metals. More details can be found in the original methods paper[67].

Dissolved metal-binding ligands

Competitive ligand exchange adsorptive cathodic stripping voltammetry (CLE-ACSV) was used to quantify the concentration and binding strength of Fe-binding organic ligands ($[L_{Fe}]_{CSV}$) in all five samples and Cu-binding organic ligands ($[L_{Cu}]_{CSV}$) in the two Southern Ocean samples. Briefly, an artificial ligand of known metal-complexation properties (salicylaldoxime) was added to samples and allowed to equilibrate with the natural ligand pool. The metal-ligand complexes are adsorbed onto a mercury drop and stripped during a cathodic sweep, generating a voltammetric signal. Voltammetric signals along a titration curve of increasing dissolved metal concentrations allow for calculation of the concentration and strengths of the natural ligand pool. Methods are described in detail elsewhere[51,72,114].

In this study, due to the high-organic and high-metal nature of fecal matter, 15–40 µL of filtered sample was diluted in 10 mL of UV-oxidized and chelexed seawater for CLE-ACSV analysis. Diluted aliquots were buffered to pH 8.2 with 50 µL of 1.5 M boric acid-ammonia buffer (Thermo Scientific), and 12.5 µL of 4 mM salicylaldoxime (Sigma-Aldrich), resulting in a final concentration of 5 µM of the artificial ligand, was pipetted into each vial and allowed to equilibrate overnight. Fe or Cu additions for the titration curve ranged from 0-100 nM (Supplementary Table 5). Differential pulse stripping voltammetry on a controlled growth mercury electrode (BASi) with a platinum auxiliary electrode and Ag/AgCl reference electrode was used for analysis, with deposition times set to 30–120 s depending on the nature of the sample and 15 s of quiet time (Supplementary Table 5).

Voltammograms for Fe and Cu titrations are given in Supplementary Fig. 2 and Supplementary Fig. 10, respectively. Peak heights were determined with a curved baseline using ECD-SOFT and input into ProMCC to calculate ligand concentrations ($[L]_{CSV}$), binding strengths ($\log K^{cond}_{FeL,Fe'}$ or $\log K^{cond}_{CuL,Cu'}$), and free metal ion ($[M']$)[115].

Dissolved humic substances

After noticing a potential humic signal on CLE-ACSV voltammograms, electroactive humic-like substances (eHS) in the Fe-ligand pool of all five fecal samples were quantified according to previously-published methods[80]. Aliquots were prepared similarly as described above, with chelexed and UV-irradiated seawater and boric acid-ammonia buffer. Additionally, 200 nM Fe and 0–300 μg L^{-1} Suwannee River Humic Acid Standard III (International Humic Substances Society) were added and allowed to equilibrate for at least 2 h. Immediately prior to running each aliquot, 0.4 M potassium bromate (ACS Grade; Neta Scientific) was added to each vial, which enhances the reduction peak for Fe-humic complexes in CSV[80]. The mercury drop electrode was operated in linear sweep mode at a -0.1 V deposition potential, 50 mV s^{-1} scan rate, and 180 s deposition time. The humic concentration was calculated from the standard addition curve (Supplementary Fig. 3) using peak areas and converted to an Fe equivalent based on the range of reported binding capacities of fulvic and humic acid standards from the Suwannee River[54,101,116].

Dissolved metallophores

To identify discrete Fe- and Cu-chelating compounds, such as siderophores, the two Southern Ocean samples were eluted from the SPE columns with methanol, dried down using a vacuum concentrator with a refrigerated vapor trap to below 1 mL (SpeedVac, Thermo Scientific), and analyzed using cutting-edge liquid chromatography (LC) coupled to both ICP-MS and electrospray ionization mass spectrometry (ESI-MS), following previously-described methods[55,57,77]. Aliquots (50 μL) were spiked with 5 μM cyanocobalamin (Sigma-Aldrich) as an internal standard and 25 μL of sample was injected onto first a ZORBAX-SB C18 trap column (0.5 × 35 mm, 5 μm; Agilent Technologies) and then a ZORBAX-SB C18 column (0.5 × 150 mm, 5 μm; Agilent Technologies) and was separated using a Dionex Ultimate 3000 LC system at a flow rate of 40 μL min^{-1} at 30 °C. The chromatography had an initial 20 min gradient from 95% solvent A (Milli-Q with 5 mM ammonium formate; Sigma-Aldrich) and 5% solvent B (methanol with 5 mM ammonium formate) to 90% solvent B, followed by a 10 min isocratic step of 90% solvent B, then a 5 min gradient from 90% to 95% solvent B, an isocratic 5 min step at 95% solvent B, and a 15 min conditioning step at 5% solvent B prior to injecting the next sample.

The LC effluent was introduced into either the ICP-MS in kinetic energy discrimination mode or the ESI-MS (Q-Exactive HF Orbitrap; Thermo Scientific), with MS1 scans collected in full positive mode with 120,000 mass resolution, 200–2000 m/z mass range, 1E6 AGC target, and 100 ms maximum injection time. MS2 scans were collected in data-dependent MS2 (dd-MS2) mode with 30,000 mass resolution, 1.0 m/z isolation window, 2E4 AGC target, 100 ms maximum injection time, 35% collision energy, and an in-house inclusion list containing the apo- and metal-bound masses of ~600 known Fe- and Cu-metallophores. Prior work[117] on siderophore characterization contains additional details.

^{56}Fe and ^{63}Cu peaks were identified in LC-ICP-MS chromatograms using custom R scripts. Individual peak areas, as well as total SPE metal-bound ligand concentrations ($[Fe\text{-}L]_{SPE}$, $[Cu\text{-}L]_{SPE}$) based on the area of the chromatogram, were calculated with standard curves of the siderophore ferrioxamine E (Supplementary Fig. 11; $R^2 > 0.99$; Sigma-Aldrich). The limit of detection for an individual peak based on the standard curve for this analysis was 8–26 pM (Supplementary Fig. 11), but large amounts of chromatographically-unresolved ligands can obscure small peaks. A small correction was applied to $[Cu\text{-}L]_{SPE}$ based on the ratio of typical Fe and Cu sensitivities in our LC-ICP-MS method. Following peak quantification, LC-ESI-MS data was used to identify masses with similar retention times as LC-ICP-MS peaks. Raw data files were converted to mzXML format using MSConvert (Proteowizard), and processing was carried out with in-house R scripts rooted in previously-published workflows[55,57,77]. For each peak, R package RaMS[118] was used to subset data structures to a time window of ±75 s of the peak's ICP-MS retention time. Then, extracted ion chromatograms (EICs) were iteratively generated in 0.005 *m/z* increments for *m/z*'s 300-1800 and a peak shape score was calculated based on the integral of the squared intensity as a function of time[77]. Candidate masses with good scores were further investigated by searching for and evaluating the peak shape of apo masses, ^{13}C isotopologues and metal isotopologues. Candidate masses were identified as metallophores by the presence of two LC-ESI-MS EIC peaks at the LC-ICP-MS retention time of a given metal, with Δ*m/z* equal to the mass difference of the two most abundant metal isotopes and intensity ratios similar to the natural abundance ratios of the two isotopes. The magnitude of differences between the measured Δ*m/z* for Cu isotopes and 1.998192, the exact Δ*m/z* for Cu ligands, in this analysis ranged from 0.008–0.292 mDa (Supplementary Tables 3-4).

After noticing a large number of novel Cu-binding compounds, samples were analyzed using LC coupled to the custom-built hybrid linear ion trap Fourier transform ion cyclotron resonance mass spectrometer (FT-ICR MS) at 21 Tesla at the National High Magnetic Field Laboratory (Tallahassee, FL, USA) to obtain ultrahigh-resolution exact masses[84]. This custom-built FT-ICR MS at 21 T is able to achieve the high mass resolving power, dynamic range, and sensitivity needed to confidently assign molecular formulae to low abundance species within a complex organic matrix[83]. Cu ligands were separated using a Dionex Ulitmate 3000 (Thermo Scientific) LC equipped with the same Zorbax-SB C18 column (0.5 × 150 mm, 5 μm) as for the LC-ICP-MS and LC-ESI-MS (Orbitrap) analyses. The LC conditions used were also replicated. The LC was directly coupled to a heated electrospray ionization source (HESI), operated in positive mode at 3.5 kV. The capillary and source heater temperatures were set to 350 °C and 75 °C, respectively. The sheath and auxiliary gas were set to 15 and 5 (arbitrary units), respectively. MS1 spectra were collected at a resolution of 1,200,000 at 400 *m/z* and an AGC target of 1×10^6 charges from 200 to 1600 *m/z*, with a maximum inject time of 500 ms. Using Freestyle (Thermo Scientific), exact masses as well as intensities of ^{13}C-, ^{15}N-, ^{18}O-, and ^{34}S-isotopologues (if present) were used to determine the putative molecular formula of the compound. If there were too few isotopologue peaks present and/or too many reasonable possibilities, no putative molecular formula was recorded. The difference between the mass observed on the FT-ICR-MS and the monoisotopic mass of the assigned formula, or the assignment error, were all below 1 ppm and averaged 0.37 ppm (Supplementary Table 3). Select ions were targeted for fragmentaiton in the ion trap using collionally induced dissociation (CID), with a normalized collisional energy of 40. MS2 spectra were collected using an isolation width of 1.6 Da.

Reporting summary

Further information on research design is available in the Nature Portfolio Reporting Summary linked to this article.

Data availability

Reported data in this study can be found in Tables S1–S3 of the supplement. LC-ESI-MS (Orbitrap) and LC-FT-ICR-MS raw data has been deposited in the Mass Spectrometry Interactive Virtual Environment (MassIVE) database and can be accessed under MSV000094994 (https://doi.org/10.25345/C50000B5D) and MSV000094995 (https://doi.org/10.25345/C5V98034P), respectively. RStudio, ChemDraw, and Thermo FreeStyle were the primary software used in this study. MetFrag (msbi.ipb-halle.de/MetFrag/) was used for the preliminary MS2 annotations in the supplement, and PubChem (pubchem.ncbi.nlm.nih.gov/) was used to pull many of the structures of known compounds. Code used to generate figures is deposited in GitHub and can be accessed under https://doi.org/10.5281/zenodo.14188098.

Received: 25 July 2024; Accepted: 13 December 2024;
Published online: 10 January 2025

References

1. Browning, T. J. & Moore, C. M. Global analysis of ocean phytoplankton nutrient limitation reveals high prevalence of co-limitation. *Nat. Commun.* **14**, 5014 (2023).
2. Coale, K. H. et al. A massive phytoplankton bloom induced by an ecosystem-scale iron fertilization experiment in the equatorial Pacific Ocean. *Nature* **383**, 495–501 (1996).
3. Boyd, P. W. et al. Mesoscale iron enrichment experiments 1993-2005: synthesis and future directions. *Science* **315**, 612–617 (2007).
4. Boyd, P. W. & Ellwood, M. J. The biogeochemical cycle of iron in the ocean. *Nat. Geosci.* **3**, 675–682 (2010).
5. Martin, J. H. Glacial-interglacial CO_2 change: the iron hypothesis. *Palaeogeography* **5**, 1-13 (1990).
6. Twining, B. S. & Baines, S. B. The trace metal composition of marine phytoplankton. *Ann. Rev. Mar. Sci.* **5**, 191–215 (2013).
7. Brand, L. E., Sunda, W. G. & Guillard, R. R. L. Reduction of marine phytoplankton reproduction rates by copper and cadmium. *J. Exp. Mar. Bio. Ecol.* **96**, 225–250 (1986).
8. Stuart, R. K. et al. Copper toxicity response influences mesotrophic Synechococcus community structure. *Environ. Microbiol.* **19**, 756–769 (2017).
9. Amin, S. A. et al. Copper requirements of the ammonia-oxidizing archaeon Nitrosopumilus maritimus SCM1 and implications for nitrification in the marine environment. *Limnol. Oceanogr.* **58**, 2037–2045 (2013).
10. Maldonado, M. T. et al. Copper-dependent iron transport in coastal and oceanic diatoms. *Limnol. Oceanogr.* **51**, 1729–1743 (2006).
11. Rafter, P. A., Sigman, D. M. & Mackey, K. R. M. Recycled iron fuels new production in the eastern equatorial Pacific Ocean. *Nat. Commun*. **8**, 1100 (2017).
12. Tagliabue, A. et al. Surface-water iron supplies in the Southern Ocean sustained by deep winter mixing. *Nat. Geosci.* **7**, 314–320 (2014).
13. Schlosser, C. et al. Mechanisms of dissolved and labile particulate iron supply to shelf waters and phytoplankton blooms off South Georgia, Southern Ocean. *Biogeosciences* **15**, 4973–4993 (2018).
14. Ellwood, M. J. et al. Distinct iron cycling in a Southern Ocean eddy. *Nat. Commun*. **11**, 825 (2020).
15. Böckmann, S. et al. Salp fecal pellets release more bioavailable iron to Southern Ocean phytoplankton than krill fecal pellets. *Curr. Biol.* **31**, 2737–2746.e3 (2021).
16. Ratnarajah, L. et al. Monitoring and modelling marine zooplankton in a changing climate. *Nat. Commun.* **14**, 564 (2023).
17. Belyaev, O., Sparaventi, E., Navarro, G., Rodríguez-Romero, A. & Tovar-Sánchez, A. The contribution of penguin guano to the Southern Ocean iron pool. *Nat. Commun.* **14**, 1781 (2023).
18. Nicol, S. et al. Southern Ocean iron fertilization by baleen whales and Antarctic krill. *Fish Fish.* **11**, 203–209 (2010).
19. Savoca, M. S. & Nevitt, G. A. Evidence that dimethyl sulfide facilitates a tritrophic mutualism between marine primary producers and top predators. *PNAS* **111**, 4157–4161 (2014).
20. Tovar-Sanchez, A., Duarte, C. M., Hernández-León, S. & Sañudo-Wilhelmy, S. A. Krill as a central node for iron cycling in the Southern Ocean. *Geophys. Res. Lett*. **34**, R884–R887 (2007).
21. Savoca, M. S. et al. Baleen whale prey consumption based on high-resolution foraging measurements. *Nature* **599**, 85–90 (2021).
22. Ratnarajah, L., Bowie, A. R., Lannuzel, D., Meiners, K. M. & Nicol, S. The biogeochemical role of baleen whales and krill in Southern Ocean nutrient cycling. *PLoS One* **9**, 1–18 (2014).
23. Roman, J. & McCarthy, J. J. The whale pump: marine mammals enhance primary productivity in a coastal basin. *PLoS One* **5**, e13255 (2010).
24. Roman, J. et al. Whales as marine ecosystem engineers. *Front. Ecol. Environ.* **12**, 377–385 (2014).
25. Rocha, R. C., Clapham, P. J. & Ivashchenko, Y. V. Emptying the oceans: a summary of industrial whaling catches in the 20th century. *Mar. Fish. Rev.* **76**, 37–48 (2014).
26. Christensen, L. B. Marine mammal populations: reconstructing historical abundances at the global scale. *Fish. Cent. Res. Rep.* https://doi.org/10.14288/1.0074757 (2006).
27. Atkinson, A., Siegel, V., Pakhomov, E. & Rothery, P. Long-term decline in krill stock and increase in salps within the Southern Ocean. *Lett. to Nat.* **432**, 100–103 (2004).
28. Laws, R. M. Seals and whales of the Southern Ocean. *Philos. Trans. R. Soc. London. B, Biol. Sci.* **279**, 81–96 (1977).
29. Surma, S., Pakhomov, E. A. & Pitcher, T. J. Effects of whaling on the structure of the Southern Ocean food web: Insights on the 'krill surplus' from ecosystem modelling. *PLoS One* **9**, e114978 (2014).
30. Smetacek, V. *Are Declining Antarctic Krill Stocks a Result of Global Warming or of the Decimation of Whales? Impacts of Global Warming on Polar Ecosystems.* xtension://mjdgandcagmikhlbjnilkmfnjeamfikk/https://www.fbbva.es/wp-content/uploads/2017/05/dat/02SMETACEKSEPARATA.pdf (2008).
31. Ruegg, K. C. et al. Are Antarctic minke whales unusually abundant because of 20th century whaling? *Mol. Ecol.* **19**, 281–291 (2010).
32. Smetacek, V. & Nicol, S. Polar ocean ecosystems in a changing world. *Nature* **437**, 362–368 (2005).
33. Kawaguchi, S. et al. Climate change impacts on Antarctic krill behaviour and population dynamics. *Nat. Rev. Earth Environ.* **5**, 43–58 (2024).
34. Savoca, M. S. et al. Whale recovery and the emerging human-wildlife conflict over Antarctic krill. *Nat. Commun.* **15**, 7708 (2024).
35. Spicer, J. I. & Saborowski, R. Physiology and metabolism of northern krill (Meganyctiphanes norvegica Sars). *Adv. Marine Biol.* **57**, 91–126 (2010).
36. Shatova, O., Wing, S. R., Gault-Ringold, M., Wing, L. & Hoffmann, L. J. Seabird guano enhances phytoplankton production in the Southern Ocean. *J. Exp. Mar. Bio. Ecol.* **483**, 74–87 (2016).
37. Wing, S. R. et al. δ^{56}Fe in seabird guano reveals extensive recycling of iron in the Southern Ocean ecosystem. *Limnol. Oceanogr.* **62**, 1671–1681 (2017).
38. Roman, J., Nevins, J., Altabet, M., Koopman, H. & McCarthy, J. Endangered right whales enhance primany productivity in the bay of fundy. *PLoS One* **11**, 1–14 (2016).
39. Alba-González, P., Álvarez-Salgado, X. A., Cobelo-García, A., Kaal, J. & Teira, E. Faeces of marine birds and mammals as substrates for microbial plankton communities. *Mar. Environ. Res.* **174**, 105560 (2022).
40. Smith, L. V. et al. Preliminary investigation into the stimulation of phytoplankton photophysiology and growth by whale faeces. *J. Exp. Mar. Bio. Ecol.* **446**, 1–9 (2013).
41. Ratnarajah, L. et al. Physical speciation and solubility of iron from baleen whale faecal material. *Mar. Chem.* **194**, 79–88 (2017).
42. Shaked, Y. & Lis, H. Disassembling iron availability to phytoplankton. *Front. Microbiol*. **3**, 123 (2012).
43. Lis, H., Shaked, Y., Kranzler, C., Keren, N. & Morel, F. M. M. Iron bioavailability to phytoplankton: an empirical approach. *ISME J.* **9**, 1003–1013 (2015).
44. Shaked, Y., Buck, K. N., Mellett, T. & Maldonado, M. T. Insights into the bioavailability of oceanic dissolved Fe from phytoplankton uptake kinetics. *ISME J.* **14**, 1182–1193 (2020).
45. Fourquez, M. et al. Chasing iron bioavailability in the Southern Ocean: insights from phaeocystis antarctica and iron speciation. *Sci. Adv.* **9**, eadf9696 (2023).
46. Pearson, H. C. et al. Whales in the carbon cycle: can recovery remove carbon dioxide? *Trends Ecol. Evol*. **38**, 238–249 (2022).
47. Gilbert, L., Jeanniard-du-Dot, T., Authier, M., Chouvelon, T. & Spitz, J. Composition of cetacean communities worldwide shapes their

contribution to ocean nutrient cycling. *Nat. Commun.* **14**, 5823 (2023).
48. Ratnarajah, L. et al. A preliminary model of iron fertilisation by baleen whales and Antarctic krill in the Southern Ocean: sensitivity of primary productivity estimates to parameter uncertainty. *Ecol. Modell.* **320**, 203–212 (2016).
49. Maldonado, M. T., Surma, S. & Pakhomov, E. A. Southern Ocean biological iron cycling in the pre-whaling and present ecosystems. *Philos. Trans. R. Soc. A Math. Phys. Eng. Sci*. **374**, 20150292 (2016).
50. Gledhill, M. & Buck, K. N. The organic complexation of iron in the marine environment: a review. *Front. Microbiol.* **3**, 1–17 (2012).
51. Campos, M. L. A. M. & van den Berg, C. M. G. Determination of copper complexation in sea water by cathodic stripping voltammetry and ligand competition with salicylaldoxime. *Anal. Chim. Acta* **284**, 481–496 (1994).
52. Ruacho, A., Richon, C., Whitby, H. & Bundy, R. M. Sources, sinks, and cycling of dissolved organic copper binding ligands in the ocean. *Commun. Earth Environ.* **3**, 1–19 (2022).
53. Hassler, C. S., Schoemann, V., Nichols, C. M., Butler, E. C. V. & Boyd, P. W. Saccharides enhance iron bioavailability to southern ocean phytoplankton. *Proc. Natl. Acad. Sci. USA.* **108**, 1076–1081 (2011).
54. Laglera, L. M. & van den Berg, C. M. G. Evidence for geochemical control of iron by humic substances in seawater. *Limnol. Oceanogr.* **54**, 610–619 (2009).
55. Bundy, R. M. et al. Distinct siderophores contribute to iron cycling in the mesopelagic at station ALOHA. *Front. Mar. Sci.* **5**, 1–15 (2018).
56. Boiteau, R. M. et al. Structural characterization of natural nickel and copper binding ligands along the US GEOTRACES eastern Pacific zonal transect. *Front. Mar. Sci*. https://doi.org/10.3389/fmars.2016.00243 (2016).
57. Boiteau, R. M. et al. Siderophore-based microbial adaptations to iron scarcity across the eastern Pacific Ocean. *Proc. Natl. Acad. Sci. USA* **113**, 14237–14242 (2016).
58. Kessler, N., Kraemer, S. M., Shaked, Y. & Schenkeveld, W. D. C. Investigation of siderophore-promoted and reductive dissolution of dust in marine microenvironments such as trichodesmium colonies. *Front. Mar. Sci.* **7**, 1–15 (2020).
59. Moffett, J. W. & Brand, L. E. Production of strong, extracellular Cu chelators by marine cyanobacteria in response to Cu stress. *Limnol. Oceanogr.* **41**, 388–395 (1996).
60. He, R. et al. SIDERITE: Unveiling hidden siderophore diversity in the chemical space through digital exploration. *iMeta* **3**, e192 (2024).
61. Babcock-Adams, L. Molecular characterization of organically bound copper in the marine environment. *Woods Hole Open Access Serv*. https://doi.org/10.1575/1912/28623 (2022).
62. Babcock-Adams, L., Li, J., McKenna, A. M., Hendrickson, C. L. & Repeta, D. J. Detection and structural elucidation of copper binding tri- and tetrapyrrole ligands produced by the marine diatom phaeodactylum tricornutum. *J. Am. Soc. Mass Spectrom*. In Review (2024).
63. Hassler, C. S. & Schoemann, V. Bioavailability of organically bound Fe to model phytoplankton of the Southern Ocean. *Biogeosciences* **6**, 2281–2296 (2009).
64. Boiteau, R. M. & Repeta, D. J. Slow kinetics of iron binding to marine ligands in seawater measured by isotope ex change liquid chromatography-inductively coupled plasma mass spectrometry. *Environ. Sci. Technol.* **56**, 3770–3779 (2022).
65. Cabanes, D. J. E. et al. Using Fe chemistry to predict Fe uptake rates for natural plankton assemblages from the Southern Ocean. *Mar. Chem*. **225**, 103853 (2020).
66. Semeniuk, D. M., Bundy, R. M., Payne, C. D., Barbeau, K. A. & Maldonado, M. T. Acquisition of organically complexed copper by marine phytoplankton and bacteria in the northeast subarctic Pacific Ocean. *Mar. Chem.* **173**, 222–233 (2015).
67. Berger, C. J. M., Lippiatt, S. M., Lawrence, M. G. & Bruland, K. W. Application of a chemical leach technique for estimating labile particulate aluminum, iron, and manganese in the Columbia river plume and coastal waters off Oregon and Washington. *J. Geophys. Res*. **113**, C2 (2008).
68. Raiswell, R., Benning, L. G., Tranter, M. & Tulaczyk, S. Bioavailable iron in the Southern Ocean: the significance of the iceberg conveyor belt. *Geochem. Trans*. **9**, 7 (2008).
69. Biller, D. V. & Bruland, K. W. Sources and distributions of Mn, Fe, Co, Ni, Cu, Zn, and Cd relative to macronutrients along the central California coast during the spring and summer upwelling season. *Mar. Chem.* **155**, 50–70 (2013).
70. Tagliabue, A. et al. A global compilation of dissolved iron measurements: focus on distributions and processes in the Southern Ocean. *Biogeosciences* **9**, 2333–2349 (2012).
71. GEOTRACES I. D. P. Group. The GEOTRACES intermediate data product 2021v2 (IDP2021v2). *NERC EDS Br. Oceanogr. Data Cent. NOC.* https://doi.org/10.5285/ff46f034-f47c-05f9-e053-6c86abc0dc7e (2023).
72. Abualhaija, M. M. & van den Berg, C. M. G. Chemical speciation of iron in seawater using catalytic cathodic stripping voltammetry with ligand competition against salicylaldoxime. *Mar. Chem.* **164**, 60–74 (2014).
73. Bundy, R. M., Biller, D. V., Buck, K. N., Bruland, K. W. & Barbeau, K. A. Distinct pools of dissolved iron-binding ligands in the surface and benthic boundary layer of the California current. *Limnol. Oceanogr.* **59**, 769–787 (2014).
74. Smith, A. J. R. et al. Identifying potential sources of iron-binding ligands in coastal Antarctic environments and the wider Southern Ocean. *Front. Mar. Sci*. https://doi.org/10.3389/fmars.2022.948772 (2022).
75. Bundy, R. M., Jiang, M., Carter, M. & Barbeau, K. A. Iron-binding ligands in the Southern California current system: mechanistic studies. *Front. Mar. Sci*. https://doi.org/10.3389/fmars.2016.00027 (2016).
76. Boye, M. et al. Organic complexation of iron in the Southern Ocean. *Deep. Res. Part I Oceanogr. Res. Pap.* **48**, 1477–1497 (2001).
77. Li, J. et al. Element-selective targeting of nutrient metabolites in environmental samples by inductively coupled plasma mass spectrometry and electrospray ionization mass spectrometry. *Front. Mar. Sci*. https://doi.org/10.3389/fmars.2021.630494 (2021).
78. Batchelli, S., Muller, F. L. L., Chang, K. C. & Lee, C. L. Evidence for strong but dynamic iron-humic colloidal associations in humic-rich coastal waters. *Environ. Sci. Technol.* **44**, 8485–8490 (2010).
79. Kinniburgh, D. G. et al. Ion binding to natural organic matter: competition, heterogeneity, stoichiometry and thermodynamic consistency. *Colloids Surfaces A. Physicochem. Eng. Asp.* **151**, 147–166 (1999).
80. Laglera, L. M., Battaglia, G. & van den Berg, C. M. G. Determination of humic substances in natural waters by cathodic stripping voltammetry of their complexes with iron. *Anal. Chim. Acta* **599**, 58–66 (2007).
81. Buck, K. N. et al. The organic complexation of iron and copper: an intercomparison of competitive ligand exchange-adsorptive cathodic stripping voltammetry (CLE-ACSV) techniques. *Limnol. Oceanogr. Methods* **10**, 496–515 (2012).
82. Lopez, J. S., Lee, L. & Mackey, K. R. M. The toxicity of copper to crocosphaera watsonii and other marine phytoplankton: a systematic review. *Front. Mar. Sci*. https://doi.org/10.3389/fmars.2018.00511 (2019).
83. Bahureksa, W. et al. Improved dynamic range, resolving power, and sensitivity achievable with FT-ICR mass spectrometry at 21 T reveals the hidden complexity of natural organic matter. *Anal. Chem.* **94**, 11382–11389 (2022).

84. Hendrickson, C. L. et al. 21 tesla fourier transform ion cyclotron resonance mass spectrometer: a national resource for ultrahigh resolution mass analysis. *J. Am. Soc. Mass Spectrom.* **26**, 1626–1632 (2015).
85. Quinn, K. D., Nguyen, N. Q. T., Wach, M. M. & Wood, T. D. Tandem mass spectrometry of bilin tetrapyrroles by electrospray ionization and collision-induced dissociation. *Rapid Commun. Mass Spectrom.* **26**, 1767–1775 (2012).
86. Meskhidze, N. et al. Perspective on identifying and characterizing the processes controlling iron speciation and residence time at the atmosphere-ocean interface. *Mar. Chem*. **217**, 103704 (2019).
87. Topalov, G. & Kishi, Y. Chlorophyll catabolism leading to the skeleton of dinoflagellate and krill luciferins: Hypothesis and model studies. *Angew. Chemie* **40**, 3892–3894 (2001).
88. Orten, J. M. Metabolism of hemoglobin and bile pigments. *Ann. Clin. Lab. Sci.* **1**, 113–124 (1971).
89. Chen, X. & Li, B. How nature incorporates sulfur and selenium into bioactive natural products. *Curr. Opin. Chem. Biol.* **76**, 1–11 (2023).
90. Pérez-Gálvez, A. & Roca, M. Phyllobilins: A new group of bioactive compounds.*Stud. Nat. Products Chem.* **52**, 159–191 (2017).
91. Li, C. & Kräutler, B. Transition metal complexes of phyllobilins—a new realm of bioinorganic chemistry. *Dalt. Trans.* **44**, 10116–10127 (2015).
92. Ponganis, P. J. Diving mammals. In *Comprehensive Physiology* 447–465 (Wiley, 2011).
93. Mochizuki, N. et al. The cell biology of tetrapyrroles: a life and death struggle. *Trends Plant Sci.* **15**, 488–498 (2010).
94. Ruacho, A. et al. Copper Ligand Production from Iron-Limited Diatoms. *Ocean Sci. Meeting* **919**, 170752 (2024).
95. Sanders, J. G. et al. Baleen whales host a unique gut microbiome with similarities to both carnivores and herbivores. *Nat. Commun.* **6**, 8285 (2015).
96. Olsen, M. A., Blix, A. S., Utsi, T. H. A., Sørmo, W. & Mathiesen, S. D. Chitinolytic bacteria in the minke whale forestomach. *Can. J. Microbiol.* **46**, 85–94 (2000).
97. Rue, E. & Bruland, K. Domoic acid binds iron and copper: a possible role for the toxin produced by the marine diatom Pseudo-nitzschia. *Mar. Chem.* **76**, 127–134 (2001).
98. Lefebvre, K. A., Bargu, S., Kieckhefer, T. & Silver, M. W. From sanddabs to blue whales: the pervasiveness of domoic acid. *Toxicon* **40**, 971–977 (2002).
99. Wells, M. L., Trick, C. G., Cochlan, W. P., Hughes, M. P. & Trainer, V. L. Domoic acid: the synergy of iron, copper, and the toxicity of diatoms. *Limnol. Oceanogr.* **50**, 1908–1917 (2005).
100. Norman, L. et al. The role of bacterial and algal exopolymeric substances in iron chemistry. *Mar. Chem.* **173**, 148–161 (2015).
101. Whitby, H. et al. A call for refining the role of humic-like substances in the oceanic iron cycle. *Sci. Rep.* **10**, 6144 (2020).
102. Hioki, N. et al. Laterally spreading iron, humic-like dissolved organic matter and nutrients in cold, dense subsurface water of the Arctic Ocean. *Sci. Rep.* **4**, 6775 (2014).
103. Paris, R. & Desboeufs, K. V. Effect of atmospheric organic complexation on iron-bearing dust solubility. *Atmos. Chem. Phys.* **13**, 4895–4905 (2013).
104. Mendez, J., Guieu, C. & Adkins, J. Atmospheric input of manganese and iron to the ocean: Seawater dissolution experiments with Saharan and North American dusts. *Mar. Chem.* **120**, 34–43 (2010).
105. Andrews-Goff, V. et al. Humpback whale migrations to Antarctic summer foraging grounds through the southwest Pacific Ocean. *Sci. Rep.* **8**, 12333 (2018).
106. Bestley, S. et al. New insights into prime Southern Ocean forage grounds for thriving Western Australian humpback whales. *Sci. Rep.* **9**, 13988 (2019).
107. Herr, H. et al. Return of large fin whale feeding aggregations to historical whaling grounds in the Southern Ocean. *Sci. Rep*. **12**, 9458 (2022).
108. Moreau, S. et al. Wind-driven upwelling of iron sustains dense blooms and food webs in the eastern Weddell Gyre. *Nat. Commun.* **14**, 9458 (2023).
109. Schine, C. M. S. et al. Massive Southern Ocean phytoplankton bloom fed by iron of possible hydrothermal origin. *Nat. Commun.* **12**, 1–11 (2021).
110. Ryan, C. et al. Commercial krill fishing within a foraging supergroup of fin whales in the Southern Ocean. *Ecology* **104**, e4002 (2023).
111. Smetacek, V., Assmy, P. & Henjes, J. The role of grazing in structuring Southern Ocean pelagic ecosystems and biogeochemical cycles. *Antarct. Sci.* **16**, 541–558 (2004).
112. Tulloch, V. J. D., Plagányi, É. E., Brown, C., Richardson, A. J. & Matear, R. Future recovery of baleen whales is imperiled by climate change. *Glob. Chang. Biol.* **25**, 1263–1281 (2019).
113. Cutter, G. A. et al. *Sampling and Sample-Handling Protocols for GEOTRACES Cruises.* https://www.geotraces.org/methods-cookbook/ (2017).
114. Rue, E. L. & Bruland, K. W. Complexation of iron(III) by natural organic ligands in the central North Pacific as determined by a new competitive ligand equilibration/adsorptive cathodic stripping voltammetric method. *Mar. Chem.* **50**, 117–138 (1995).
115. Omanović, D., Garnier, C. & Pižeta, I. ProMCC: An all-in-one tool for trace metal complexation studies. *Mar. Chem.* **173**, 25–39 (2015).
116. Sukekava, C., Downes, J., Slagter, H. A., Gerringa, L. J. A. & Laglera, L. M. Determination of the contribution of humic substances to iron complexation in seawater by catalytic cathodic stripping voltammetry. *Talanta* **189**, 359–364 (2018).
117. Park, J. et al. Siderophore production and utilization by marine bacteria in the North Pacific Ocean. *Limnol. Oceanogr.* **68**, 1636–1653 (2023).
118. Kumler, W. & Ingalls, A. E. Tidy data neatly resolves mass-spectrometry's ragged arrays. *R. J.* **14**, 193–202 (2022).
119. Rivas-Ubach, A. et al. Moving beyond the van Krevelen diagram: a new stoichiometric approach for compound classification in organisms. *Anal. Chem.* **90**, 6152–6160 (2018).

Acknowledgements

The authors thank Marion Fourquez, Sylvia Sander, and one anonymous reviewer for their helpful comments during review of this manuscript. P.J.M. was supported in this work under the MUIR Program at the Stanford Woods Institute for the Environment, the Program on Climate Change at the University of Washington, and a Ford Foundation Predoctoral Fellowship. M.S.S. was supported by MAC3 Impact Philanthropies. J.A.R. was supported by NOAA-PMEL's Earth-Ocean Interactions Program (PMEL publication #5672) through the University of Washington's Cooperative Institute for Climate, Ocean, and Ecosystem Studies (CICOES publication #2024-1397). Authors thank Jakub T. Sliwinski with the TraceLab at the University of Washington School of Oceanography for assistance in acquiring trace metal data. We also acknowledge Anitra E. Ingalls, Laura Truxal, and Jiwoon Park at the University of Washington School of Oceanography in acquiring Orbitrap ESI-MS data and members of the National High Magnetic Field Laboratory for assistance with acquiring FT-ICR-MS data. The National High Magnetic Field Laboratory is supported by the National Science Foundation Division of Materials Research and Division of Chemistry through DMR-1644779 and the State of Florida. We also thank Anitra E. Ingalls for helpful comments on the manuscript. Samples collected in the Antarctic were supported by the National Science Foundation Office of Polar Programs (ANT-1643877) and the Palmer Long Term Ecological Research Program (ANT-1440435, ANT-2026045) under ACA Permits 2015-011 and 2020-016 to A.S.F. CRC samples were collected under NOAA research permit #21678 issued to J.C. We acknowledge James A. Fahlbusch in sampling efforts for CRC samples.

Author contributions

P.J.M conducted project formulation, laboratory and data analyses, and manuscript preparation. M.S.S. provided samples, provided project

mentorship, and assisted manuscript preparation. L.B.A. conducted FT-ICR-MS analyses, assisted with MS data analysis and interpretation, and assisted manuscript preparation. L.E.M. assisted with LC-ICP-MS and LC-ESI-MS analyses. A.R. and D.H. conducted chemical leaches. L.J.P., R.C.N., J.C., A.S.F., J.G., and M.S.S. conducted and/or organized sample collection. J.A.R. and R.M.B provided project mentorship and assisted manuscript preparation. All co-authors were involved in editing manuscript or have read and approved manuscript.

Competing interests
The authors declare no competing interests.

Additional information
Supplementary information The online version contains supplementary material available at https://doi.org/10.1038/s43247-024-01965-9.

Correspondence and requests for materials should be addressed to Patrick J. Monreal or Randelle M. Bundy.

Peer review information *Communications Earth & Environment* thanks Marion Fourquez, Cristina Genovese and Sylvia Sander for their contribution to the peer review of this work. Primary Handling Editors: Alice Drinkwater. A peer review file is available.